

Interaction of a HVDC System with 400-kV AC Systems on the Same Tower

M. Kizilcay, A. Agdemir, M. Lösing

Abstract—The loading of existing power systems will in the near future further increase for example because of increasing demands and difficulties to open new transmission corridors. Parallel operation of a bipolar high-voltage direct-current (HVDC) power transmission system with the 400-kV alternating-current (AC) power transmission systems on the same line route can be seen as one of the solutions for increasing of power transmission capability and avoid of system stability problems. One consequence such an application is various AC/DC interaction phenomena and system reliability problems. This paper presents the results of HVDC/AC power transmission system interactions for the selected hybrid tower configuration.

Keywords: HVDC transmission, electromagnetic coupling, HVDC/AC interaction model, AC/DC hybrid transmission, power systems fault, secondary arc, electromagnetic transient.

I. INTRODUCTION

High-voltage direct-current (HVDC) transmission power systems are more advantageous than high-voltage AC transmission systems over long distances in consideration of the reduced voltage drops and the lower operating costs. One possibility could be to add a HVDC system to an existing AC transmission system. Alternatively an existing AC system can be replaced by a HVDC system on the same tower. The multi-system (AC/DC hybrid transmission) would increase the power transmission capacity of a transmission corridor [1]. The disadvantage resulting from the hybrid power transmission on the same tower is the significant coupling at fundamental frequency from the AC transmission system to the HVDC transmission system or likewise the HVDC system can also affect the AC system under certain system conditions or failure. Interaction and coupling problems between HVDC and AC transmission systems have been discussed in the previous papers [1]-[9].

Based on the first CIGRÉ HVDC benchmark system [10] and on the available model of that monopolar system [11],

a bipolar ± 500 kV HVDC system has been modeled using the graphical preprocessor ATPDraw and EMTP-ATP [12]. The bipolar HVDC model comprises positive and negative pole. Each pole includes twelve-pulse converter units, their control systems, smoothing reactors, converter transformers and AC filters at the rectifier and inverter side. The bipolar HVDC model and control system techniques have been described in detail in [13].

The tower layout selected for the parallel operation of the HVDC and AC systems is shown in Fig. 1. The AC systems are numbered 1, 2 and 3 and the phase sequence of the three-phase AC systems is also shown. The HVDC power transmission system consists of three bundle-conductors for positive and negative poles, and return conductor K (right-upper conductors in Fig. 1). The AC and DC transmission systems shown are represented as a multi-phase conductor system with sub-conductors with the LINE CONSTANTS program of EMTP-ATP. At first stage a basic configuration of a 300-km long line route has been modeled and the interaction of the HVDC and AC systems has been analyzed. At the second stage a more realistic transmission power system will be modeled and analyzed. The investigations of the first stage consist of steady-state and transients computations of the following phenomena:

- Fundamental frequency coupling on the DC line
- DC component coupling on disconnected AC lines
- Effect of the AC system faults (single-phase, phase-to-phase, three-phase, etc.) on the DC line
- Effect of the DC line faults on the AC lines
- Energization of the AC and DC transmission systems
- Loss of a pole during HVDC bipolar operating
- Secondary arc effects of AC/DC hybrid line

This study focuses on the electromagnetic coupling and interaction of the AC and DC lines on the same tower.

II. SYSTEM REPRESENTATION IN THE EMTP-ATP

Fig. 2 shows the modeled hybrid AC/DC systems. The total transmission length is 300-km. Each AC system is rated at 400 kV, 50 Hz, 1700 MVA and the HVDC system is a bipolar ± 500 kV, 2600 MW. Damped a low frequency and a high-frequency AC filters are added to absorb the harmonics generated by the converter as well as together with a fixed shunt capacitor to supply reactive power to the converter.

M. Kizilcay is with the Department of Electrical Eng. and Computer Science, University of Siegen, Siegen, Germany

(email of corresponding author: kizilcay@uni-siegen.de).

A. Agdemir is with the Department of Electrical Eng. and Computer Science, University of Siegen, Siegen, Germany

(email: aykut.agdemir@uni-siegen.de)

M. Lösing is with the RWE Transportnetz Strom, Dortmund, Germany
(email: martin.loesing@rwe.com)

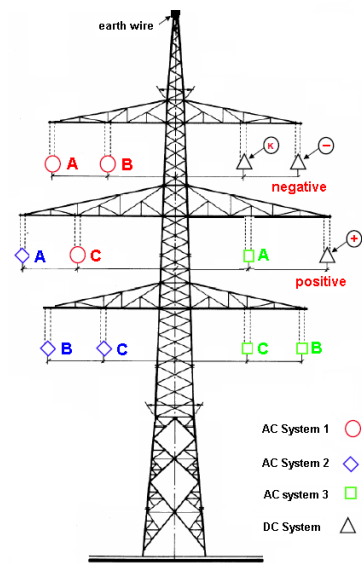


Fig. 1. The hybrid AC/DC tower layout

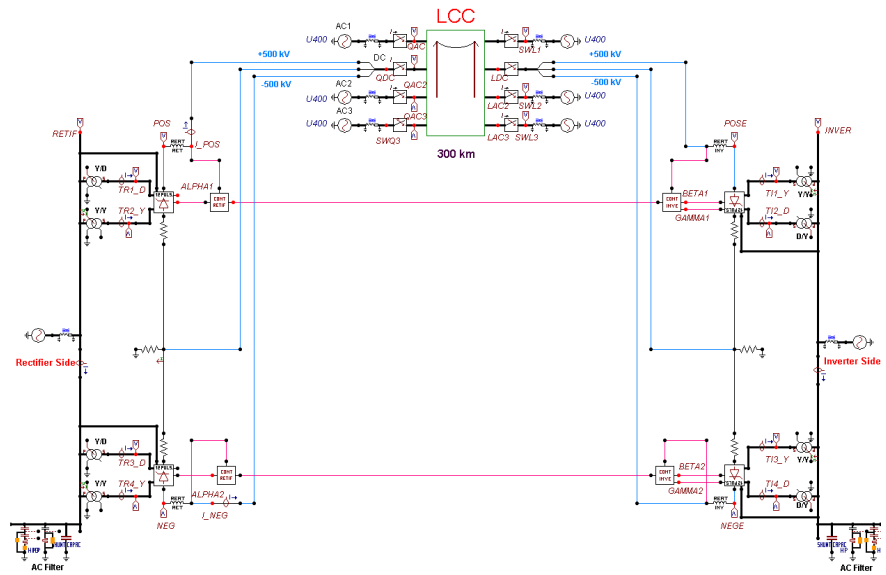


Fig. 2. Simulation model in EMTP-ATP: ± 500 -kV bipolar HVDC system and three 400-kV AC circuits

The first CIGRÉ HVDC benchmark model including controller settings has been tested and evaluated at the parity simulator of FGH testing laboratory in Germany [10], [11]. The main settings of the controllers without any change are used in the study for the modelling of the bipolar HVDC system.

The twelve-pulse converter units at the rectifier and inverter side are modelled with two six-pulse bridges in series. In the converter model, each of the six valves of the six-pulse bridge is modelled in EMTP-ATP using TACS-controlled Type-11 switch as thyristor. Series RC-snubber circuits are connected in parallel with each valve. The twelve-pulse converter unit includes a phase-locked loop (PLL) and extinction angle (γ) measurement described in MODELS language in EMTP-ATP. A phase-locked-loop (PLL) is used to generate three voltages synchronized on the fundamental frequency component of the positive-sequence voltages.

Since a DC system embedded in a AC system cannot be taken into consideration in the steady-state phasor solution of EMTP-ATP, an initialising scheme has been developed based on [11], which allows to start the simulation from a steady-state solution for the coupled configuration of a DC line on the same tower with the AC overhead lines at the power frequency. The DC line can be started to operate at any time after $t = 0$.

The control systems of DC voltage and line current are described in [10], [11], [13]. The DC voltage variation with delay angle α is used to regulate the DC current to its set-point. The rectifier control system uses constant-current-control technique. The inverter control has both constant-current and gamma (extinction angle) controller operating in parallel and from these two controls the minimum delay angle α is used to generate the firing pulses for the inverter valves.

III. RESULTS OF THE STUDY

The steady-state and transient interaction of the bipolar HVDC system and AC systems has been analyzed by means of digital simulations. The HVDC and AC systems are on the same tower and are operated parallel along a length of 300-km. The Pi-section line model is used for all steady-state computations and the constant-parameter distribution (Bergeron) line model for transient studies. The results of the Bergeron line model are compared with the frequency-dependent line model developed by J. R. Marti. In the paper only the results with Bergeron line model are presented because J. R. Marti model produces very similar results. The earth is assumed to be homogeneous with a resistivity, $\rho = 100 \Omega \cdot \text{m}$.

A. Fundamental Frequency Coupling on the HVDC

Fig. 3 and Fig. 4 show the coupled fundamental frequency voltage and current components on the HVDC line when the AC systems are in steady state. As an example, “AC Systems 1-2” on the x-axis in Fig. 3 and Fig. 4 means that the AC lines 1 and 2 are connected (energized) and only the AC system 3 is disconnected (de-energized) at both ends. It can be seen in those figures that the maximum root-mean-square (rms) value of the fundamental frequency voltage and current are coupled on the negative conductor reaching almost 2.5 kV and 30 A. It is observed also the coupled voltage and current due to electromagnetic coupling effect between HVDC and AC lines is in the case of “AC System 3” (only AC system 3 is in operation) higher than the other cases, because AC system 3 is the nearest system to the HVDC line at the tower (see Fig. 1). The lowest coupled fundamental frequency voltage and current are observed in the case of “AC System 1” (only AC-system 1 is in operation).

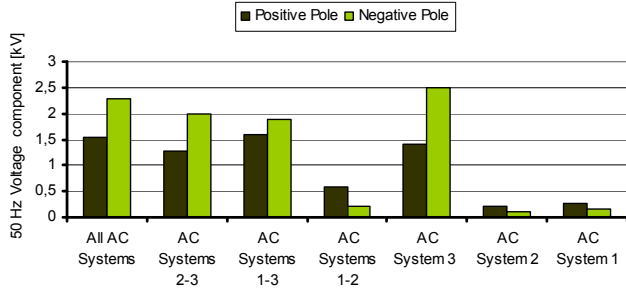


Fig. 3. The coupled fundamental frequency voltage on the wires of DC poles

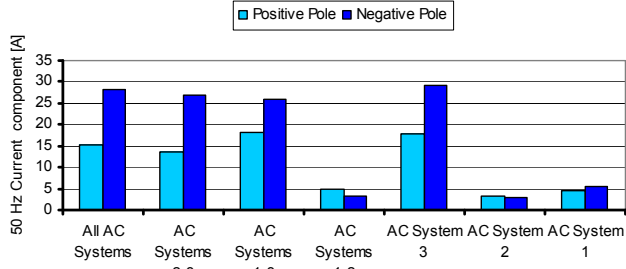


Fig. 4. The coupled fundamental frequency current on the wires of DC poles

Fig. 5 and Fig. 6 show the resulting rms values of the fundamental frequency voltage and current of the HVDC line when one phase of the AC line at the sending end is in the phase-to-ground fault state. The simulation is started from the steady-state fault conditions. The highest value of fundamental frequency voltage and current are expected in case of a single-phase-to-ground fault in phase B of AC system 3 on the positive pole of HVDC line. The values reach almost 10 kV and 95 A. A single-phase-to-ground fault in phase A of AC system 2 causes the lowest voltage and current coupling on the positive pole of HVDC. The three-phase-faults were simulated; too, the coupled fundamental voltage and current values were lower compared to a single-phase-to-ground fault.

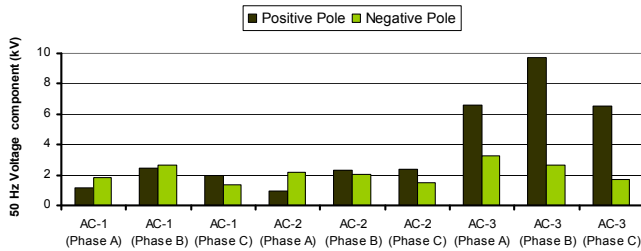


Fig. 5. Coupled fundamental frequency voltage on the wires of DC poles in case of a single-phase-to ground fault on an AC line

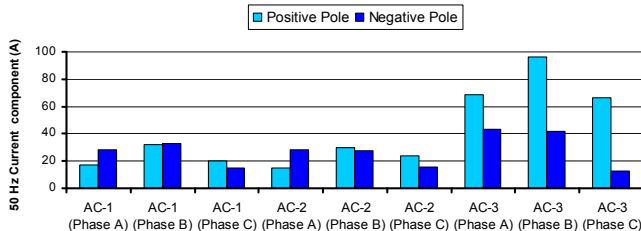


Fig. 6. Coupled fundamental frequency current on the wires of DC poles in case of a single-phase-to ground fault on an AC line

B. DC Coupling on Disconnected AC Lines

Fig. 7 shows the coupled DC voltage and fundamental frequency rms voltage values on the AC lines when one phase of an AC line is disconnected at both sides. The highest value of the fundamental frequency voltage is 75 kV for the disconnected phase B of the AC system 1. The highest DC component voltage of 55 kV is expected for the disconnected phase B in the AC system 3. Further, a negative DC voltage is coupled on the AC system 1, because AC system 1 is the nearest system to the wire of the negative DC pole.

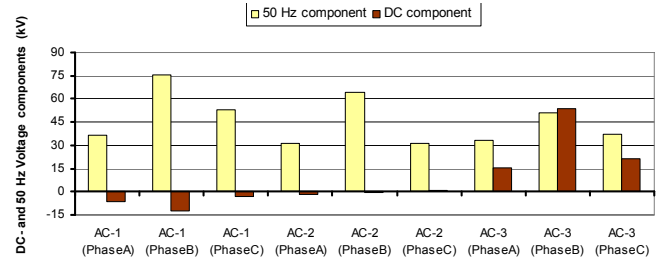


Fig. 7. Coupled DC and fundamental frequency voltage on the AC lines, due to disconnection of one phase in each AC system

C. Effects of the AC System Faults on the DC Line

The following faults in the AC system 3 (the nearest AC system to the HVDC at the tower) are simulated dynamically and the results are compared.

- single-phase-to-ground
- phase-to-phase-to-ground
- phase-to-phase
- three-phase
- three-phase-to-ground

A single-phase-to-ground fault is the worst case regarding the coupled fundamental frequency voltage and current on the DC line. The location of the fault is selected along the length of 300-km line at the sending end, receiving end and in the midpoint of the line. Fig. 8 and Fig. 9 depict the waveforms of the resulting DC voltage and current for a single-phase-to-ground fault at the sending end of the AC system 3 in phase B. The fault occurs at $t = 0.6$ s. It is observed that the delay angle of the rectifier side on the positive pole of HVDC line increases from its pre-fault nominal value 17° to 34° and the extinction angle increases from its pre-fault value 15° to 23° . The transient interaction due to coupling of the AC and DC lines can be seen in those figures. The transients in the DC voltages and currents due to sudden fault show no significant difference from the steady-state. This behaviour is also observed for DC system operation with less DC power transmission, for example 10% or 25% of the rated power.

The effect of the clearing of AC faults with the opening of the faulted AC line is also simulated and analysed. It could be seen that the influence of the AC lines on the DC lines in these cases is negligible.

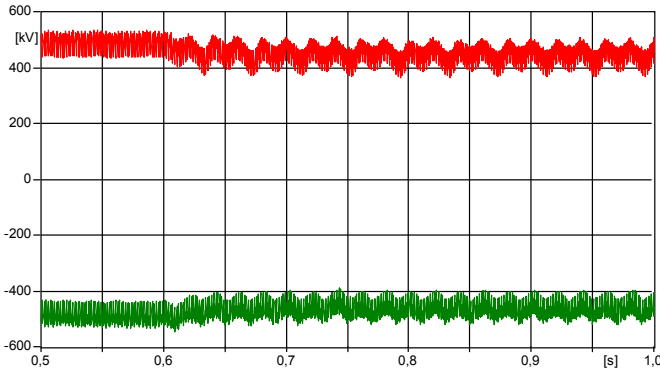


Fig. 8. Voltage of the DC line (pos. and neg. poles) in case of a single-phase-to-ground fault in phase B of the AC system 3

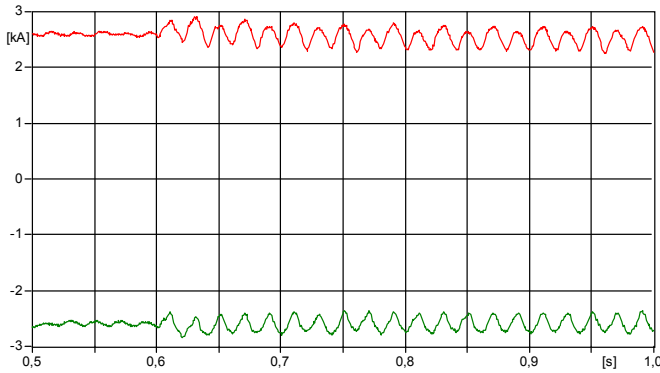


Fig. 9. Current of the DC line (pos. and neg. poles) in case of a single-phase-to-ground fault in phase B of the AC system 3

D. Effect of the DC Line Fault on the AC Lines

A DC line-to-ground fault is chosen to occur at the rectifier end behind the smoothing reactor on the positive pole wire of HVDC line as worst case. Fig. 10 shows the current flowing in the DC line. The fault occurs at $t = 0.6$ s. After a transient response of the positive pole of HVDC line the current in this pole decreases to zero. The return of the unbalanced DC current (only negative pole in operation) through the DC return conductor, the earth and AC lines is effected by the grounding of the DC return conductor at the rectifier and/or inverter side.

Through the sudden occurrence of the DC line-to-ground fault the voltage in phase A of the AC system 3 attains temporarily a peak value of 420 kV (Fig. 11).

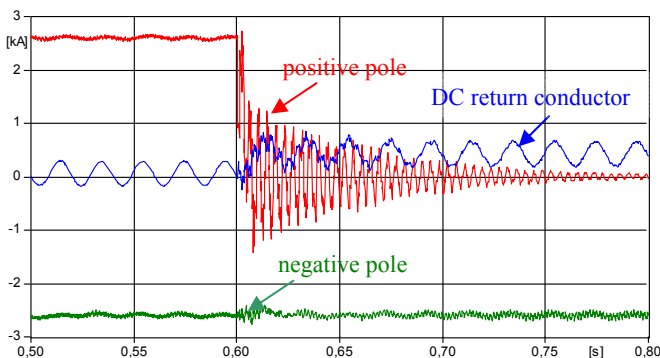


Fig. 10. Current waveforms in the DC line for a DC line-to-ground fault on the positive pole wire behind the fault location (DC return conductor grounded at both ends)

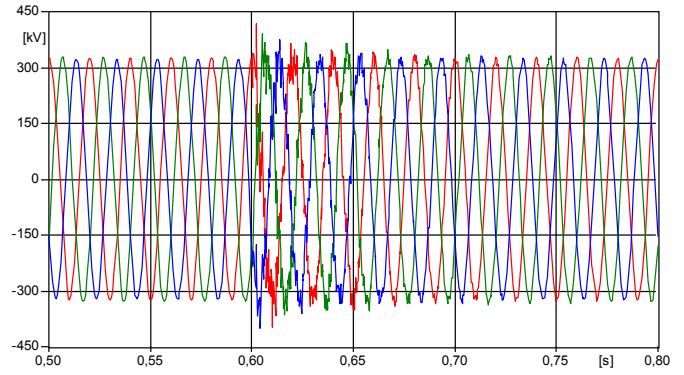


Fig. 11. Voltage of the AC system 3 for a DC line-to-ground fault at $t = 0.6$ s

E. Energization of AC and DC Transmission Lines

The following worst case is chosen for the energization of the AC system. The AC system 3 is energized at $t = 0.68$ s, when the receiving end of the AC single-line phase B is in the phase-to-ground fault state. The receiving ends of the other phases are open (phase A and C). Fig. 12 shows the AC voltage waveforms of AC system 3 at the sending end. Phase A reaches directly after the energization of the AC system a peak value of approx. 460 kV. Fig. 13 and Fig. 14 show the DC voltage and current, respectively. The coupled power frequency rms voltage and current values of the positive pole of HVDC line are 23 kV and 210 A. The energization of the DC line has negligible impact on the AC lines. If the AC system 3 will be opened at both ends of the transmission line, then the AC line is charged to a peak value of 150 kV.

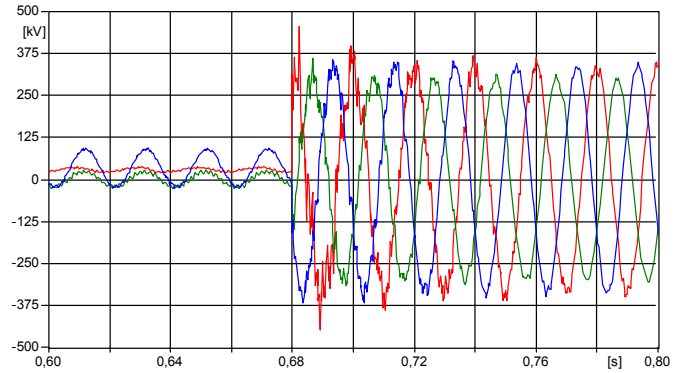


Fig. 12. Voltage of the AC system 3 in case of energization of AC system 3 with a sustaining ground fault in phase B

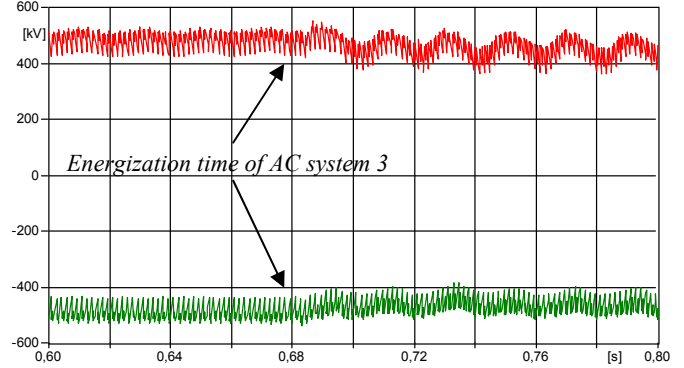


Fig. 13. Voltage of the DC lines (pos. and neg. poles) in case of energization of AC system 3

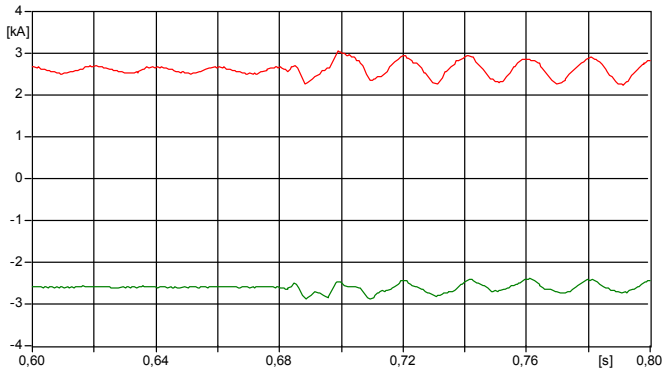


Fig. 14. Current of the DC lines (pos. and neg. poles) in case of energization of AC system 3

The spectrum of the harmonic contents of the current peak values in the converter transformer at the rectifier side (Y/Y) is shown in worst case of energization of AC system 3 (Fig. 15). A power frequency current following in the DC side of converter causes the DC and second harmonic currents in the secondary winding of the converter transformer. A small DC component in the converter transformer can impact the overall power system, particularly if the converter rating is large. The DC component offsets the converter transformer flux to cause saturation. This saturation injects a broad spectrum of harmonics into both AC and DC side [4]. To prevent flowing of power frequency currents a blocking filter on the DC line at both sides should be used. The blocking filter avoids saturation of the converter transformers in this case.

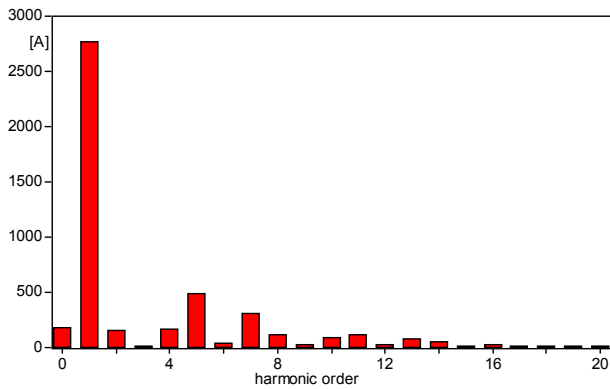


Fig. 15. Harmonic contents (peak value) of the current in the converter transformer at the rectifier side (secondary winding)

F. Loss of a Pole during HVDC bipolar operating

A simple interrupter model with active commutation principle is used for the disconnection of a pole of the HVDC line during bipolar operation. A series inductance and pre-charged capacitor are connected across the interrupter (Fig. 16). After the main interrupter on the DC line is open, another auxiliary switch is triggered to start the capacitor discharging to create oscillatory current superimposed to the interrupter current that is ultimately forced into the artificial zero crossing [14].

The DC current of the positive pole is interrupted in this

case at both ends of the DC line at $t = 0.8$ s. In Fig. 17 the resulting waveforms of the DC current are shown for the case that DC return conductor is grounded at both rectifier and inverter side. In this case a substantial part of the DC return current flows in the earth (Fig. 17). Part of the DC return current flows through the AC lines depending neutral point treatment of the AC system. The highest DC component in the phase currents is expected in the AC system 3 after the interruption of the DC positive pole current. The mean DC component of phase B current increases from -15 A to 216 A after the interruption of DC positive pole current (see Fig. 18). In phase B of the AC system 3 a temporary overvoltage of 362 kV (peak value) is observed. When the DC return conductor is grounded only at the inverter side, major part of the DC return current flows through the DC return conductor as shown in Fig. 19. In this case mean DC component of phase B current (AC system 3) amounts only to 13 A after loss of the DC positive pole.

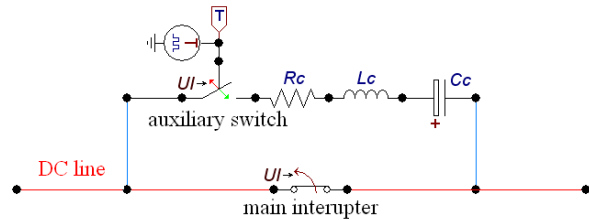


Fig. 16. DC interrupter ($R_c=1.5 \Omega$, $L_c=1.2$ mH and $C_c=1 \mu\text{F}$)

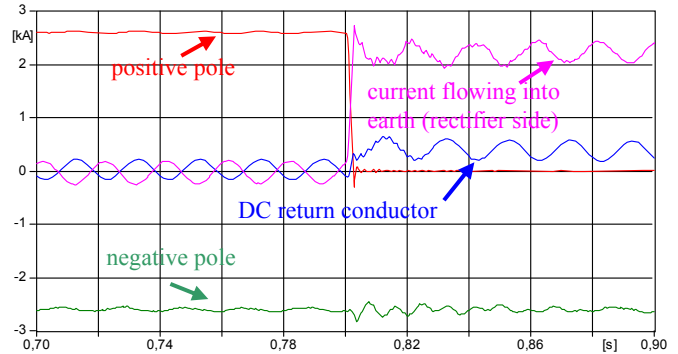


Fig. 17. Current of the DC lines (pos. and neg. poles) in case of the interruption of the DC positive pole current (DC return conductor at the both ends grounded)

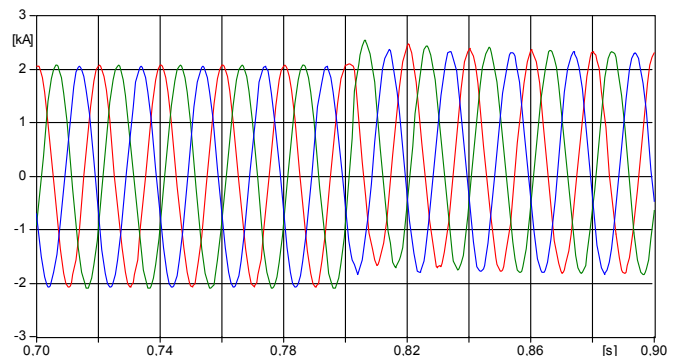


Fig. 18. Current of the AC system 3 in case of interruption of DC positive pole current (DC return conductor at the both side grounded)

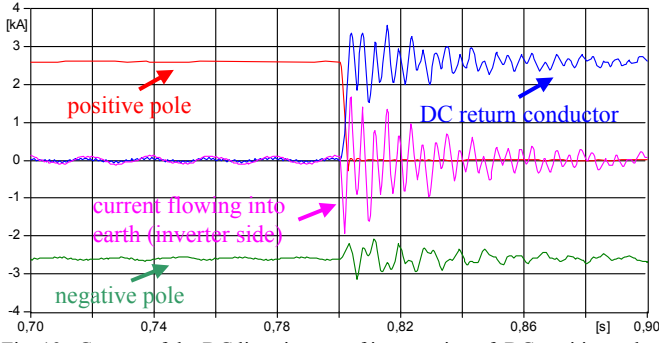


Fig. 19. Current of the DC lines in case of interruption of DC positive pole current (DC return conductor only at the inverter side grounded)

G. Secondary Arc Effects in AC/DC Hybrid Lines

Primary arc is effective after fault inception till single-phase tripping of the faulty phase. Secondary arc follows the primary arc after isolating the fault by single phase tripping on a transmission line. The power system transients caused by arcing fault are simulated and the following secondary arc effects in AC/DC hybrid transmission system are investigated:

- The effect of the coupling from the AC systems to the fault arc on the HVDC transmission system
- The effect of the coupling from the HVDC system to the secondary arc on the AC transmission systems

A dynamic arc model used in this work is based on the energy balance of the arc column and describes an arc in air by a differential equation of the arc conductance g [15], [16], [17]. The arc model relates the rate of change of the conductance with the arc current and voltage. The existing arc conductance g with dg/dt is aiming its stationary end value G .

$$\frac{dg}{dt} = \frac{1}{\tau}(G - g) \quad (1)$$

where τ : is the arc time constant,
 g : instantaneous arc conductance,
 G : stationary arc conductance.

The stationary arc conductance is defined as:

$$G = \frac{|i_{arc}|}{u_{st}} \quad (2)$$

with

$$u_{st} = u_0 + r_0 \cdot |i_{arc}| \quad (3)$$

where i_{arc} : instantaneous arc current,
 u_{st} : stationary arc voltage,
 u_0 : characteristic arc voltage,
 r_0 : characteristic arc resistance.

Parameters u_0 and r_0 are dependent on arc length l_{arc} and calculated by the following equations obtained from arc measurements [18]:

$$u_0 = 0.9 \frac{\text{kV}}{\text{m}} \cdot l_{arc} + 0.4 \text{ kV} \quad (4)$$

$$r_0 = 40 \frac{\text{m}\Omega}{\text{m}} \cdot l_{arc} + 8 \text{ m}\Omega \quad (5)$$

Equation (1) is a generalized arc equation that is suitable to represent an arc between two terminals in an electric circuit. The length of the primary arc is considered to be constant. A linear time-varying elongation of the secondary arc is taken into account by the model. In reality the arc length variation is highly dependent on external factors like wind, thermal buoyancy. The arc time constant τ is assumed to be constant during the primary arc. The time constant of the secondary arc is time varying and can be expressed as a function of arc elongation.

$$\tau = \tau_0 \cdot \left(\frac{l_{arc}}{l_0} \right)^\alpha \quad (6)$$

where τ_0 : initial time constant,
 l_0 : initial arc length,
 α : coefficient of negative value.

The arc is described in MODELS language of EMT-ATP [17], [20]. Inputs to arc model are Thevenin voltage v_{th} and resistance r_{th} at the terminals for the current time step (Fig. 20). The arc model calculates the value of the resulting arc current i_{arc} . At each time step first the stationary arc voltage u_{st} and time constant τ are updated using (3), (4), (5) and (6), which depend on instantaneous arc length l_{arc} .

The arc self-extinction phenomenon is not known in detail. There are two different approaches that try to explain arc extinction: 1) based on thermal instability described by arc equation (1). The arc extinguishes, if the time derivative of instantaneous arc resistance, dr_{arc}/dt , exceeds a pre-defined limit provided arc conductance g' per length is less than g'_{min} . 2) based on dielectric phenomenon [18]. The following limiting values per arc length are determined empirically:

$$g'_{min} = 50 \mu\text{S} \cdot \text{m}; \quad \frac{dr_{arc}}{dt} = 20 \text{ M}\Omega / (\text{s} \cdot \text{m})$$

The inductive and capacitive coupling of the power frequency from the AC transmission to the HVDC system interferes with the clearing of a DC line fault. Though DC current in the fault arc can be brought to zero by the DC interrupter, the inductive and capacitive coupling to AC systems can delay the DC arc extinction [19].

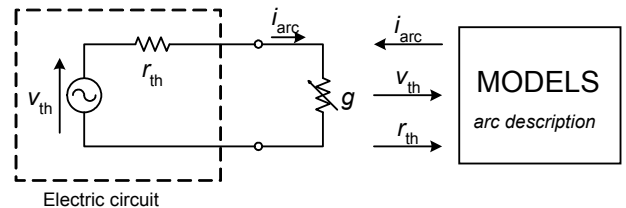


Fig. 20. Interaction between the electric circuit and the arc represented by Thevenin-type component.

Following parameters for the line-to-ground fault arc across the DC insulator are used in the arc model: $\tau_0 = 1 \text{ ms}$, $\alpha = -0.4$, $l_0 = 6 \text{ m}$

The initial arc length is assumed to be 6 m. The simulation is started from the steady-state no fault conditions. The line-to-ground fault occurs for the worst location at the rectifier end on wire of the DC positive pole. An extra 1Ω grounding resistance is included in the fault path. The fault arc is initiated at $t = 0.3 \text{ s}$. The positive pole of HVDC line is disconnected by DC interrupter at both line ends at $t = 0.5 \text{ s}$. From this moment on the secondary arc will be active.

Fig. 21 and Fig. 22 show the secondary arc voltage and current waveforms, respectively. In Fig. 20 all AC systems of the hybrid AC/DC system are in operation (case 1). In Fig. 22 the resulting waveforms of the secondary arc voltage and current with all AC lines de-energized are shown (case 2). It is observed from the simulation results of these two cases that the secondary arc duration in the case 1 is longer than in the case 2 due to the power frequency coupling from the AC systems. When the secondary arc voltage reaches the level of recovery voltage, the arc extinguishes. The secondary arc duration of 0.24 s is determined from Fig. 21. After the arc extinction at $t = 0.82 \text{ s}$ the recovery voltage in Fig. 21 has a fundamental frequency peak value of 20 kV.

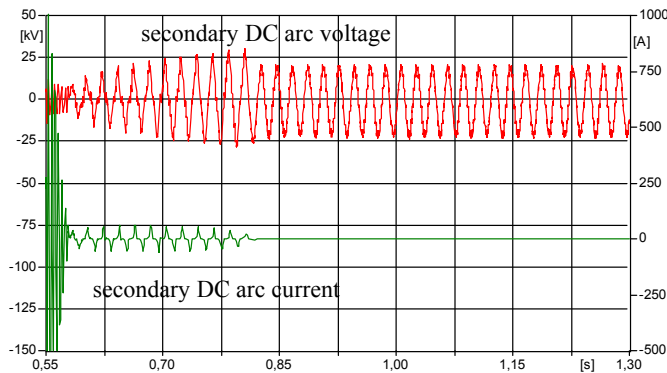


Fig. 21. Secondary arc current and voltage in case of DC line-to-ground fault, AC systems are in operation (case 1)

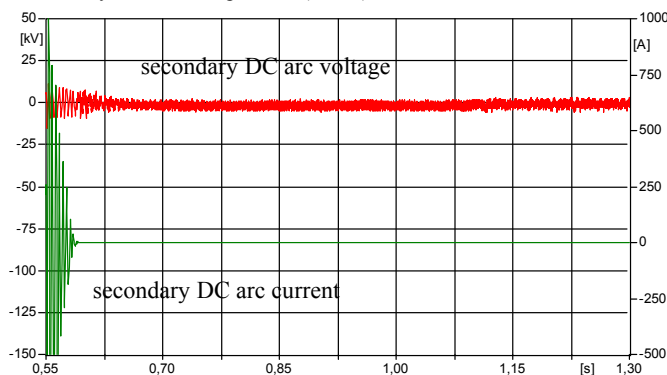


Fig. 22. Secondary arc current and voltage in case of DC line-to-ground fault, AC systems are de-energized (case 2)

Fig. 23 shows the resulting secondary arc voltage and current of the positive pole of HVDC line, if the phase B of the AC system 3 is line-to-ground faulted (case 3). It can be seen that in the case-3 the duration of secondary arc (0.6 s) is

longer and the value of secondary arc current higher than the other both cases 1 and 2. A simultaneous double ground fault on the DC and AC lines is rare in the reality. This case is chosen to show the impact of the AC system on secondary arc on the DC line.

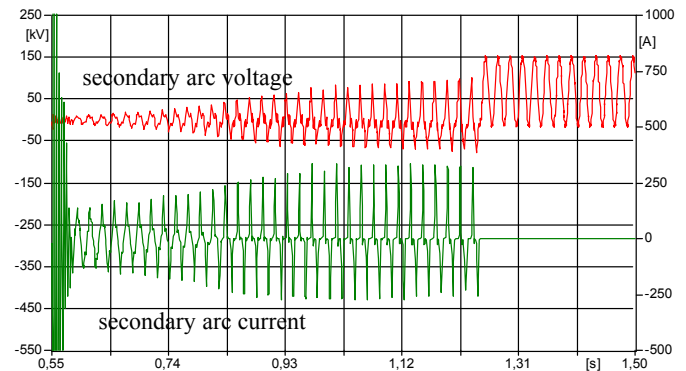


Fig. 23. Secondary arc current and voltage in case of DC line-to-ground fault, AC systems are active and a single-phase-to-ground fault in phase B of AC system 3 (case 3)

The secondary arc voltage and current of the AC system 3 in phase B are compared with and without operation of the HVDC system to study the coupling effect from the HVDC system on the secondary arc in the AC system.

Following parameters for the line-to-ground fault arc across the AC insulator (length 3.5 m) are used in the arc model: $\tau_0 = 1 \text{ ms}$, $\alpha = -0.4$, $l_0 = 3,5 \text{ m}$

As worst case the ground fault is assumed to occur in phase B of the AC system 3. The primary arc is initiated at $t = 0.1 \text{ s}$. The pole of phase B of AC circuit breakers at both line ends opens at $t = 0.3 \text{ s}$. Fig. 24 and Fig 25 show the computed arc voltage and current waveforms with and without operation of the HVDC line. Compared to the case HVDC system de-energized the secondary arc current and recovery voltage of the case with HVDC system in operation are not considerably higher resulting in a long secondary arc duration. Further simulations of the secondary arc in the other AC systems showed no significant effect of the HVDC system on secondary arc extinction and duration.

IV. CONCLUSION

The AC and DC lines on the same tower can be effectively used to increase the power transmission capacity of an existing transmission corridor. There is a number of technical questions for the parallel operation of those hybrid lines. Several issues related mainly to the inductive and capacitive coupling between DC and AC systems are investigated in this paper.

A hybrid AC/DC system on the same tower is modeled in EMT-P-ATP and the results of the steady-state and transient interaction between the AC and DC transmission lines are shown.

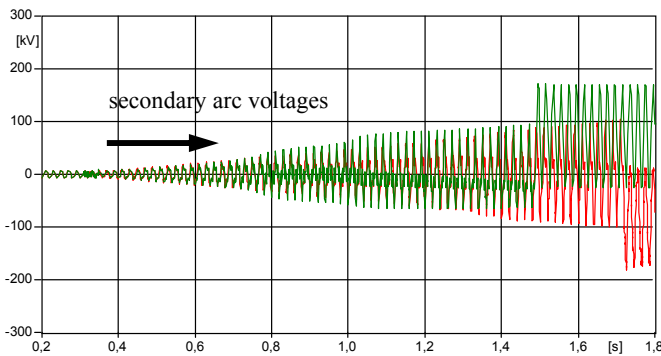


Fig. 24. Secondary arc voltage in phase B of AC system 3 with HVDC (red curve) and without HVDC transmission system (green curve)

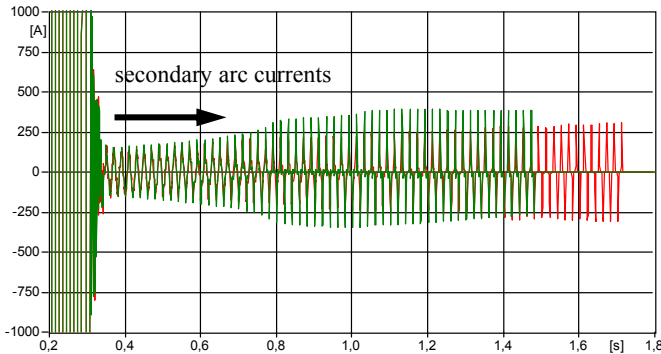


Fig. 25. Secondary arc current in phase B of AC system 3 with HVDC (red curve) and without HVDC transmission system (green curve)

The mutual interaction of the DC and AC systems is not negligible, but it is not critical that the parallel operation would become technically infeasible. At the next step an existing more complex transmission system will be considered, where the replacement of certain AC circuits by HVDC lines will be investigated by digital simulations.

V. REFERENCES

- [1] Douglas A. Halamay, Katrina M. Saxby, Juan. L. Bala, Jr., and R. Spacek, "Feasibility study of a high-voltage DC & AC multi-circuit hybrid transmission line," in *Proc. 37th Annual North American Power Symposium 2005*, Oct. 23-25, pp. 310 – 316.
- [2] R. Verdolin, A. M. Gole, E. Kuffel, N. Diseko, and B. Bisewski, "Induced overvoltages on an ac-dc hybrid transmission system," *IEEE Trans. Power Delivery*, vol. 10, no. 3, pp. 1514-1524, July 1995.
- [3] B. Gustavsen, G. Irwin, R. Mangalrød, D. Brandt, K. Kent, "Transmission line models for the simulation of interaction phenomena between parallel ac and dc overhead lines," *IPST'99, International Conference on Power Systems Transients*, Budapest-Hungary, June, 1999.
- [4] E.V. Larsen, R. A. Walling, C.J. Bridenbaugh, "Parallel AC/DC transmission lines steady-state induction issues", *IEEE Trans. Power Delivery*, vol. 4, no. 1, pp 667-674, January 1989.
- [5] J. Ulleryd, M. Ye, and G. Moreau, "Fundamental frequency coupling between HVAC and HVDC lines in the Quebec-New England multiterminal system - Comparison between field measurement and EMTDC simulations," in *Proc. Int. Conf. Power Systems Technology*, Beijing China, Aug. 18-21, 1998.
- [6] P. Sarma Maruvada, S. Drogi, "Filed and ion interactions of hybrid AC/DC transmission lines," *IEEE Trans. Power Delivery*, vol. 3, no. 3, pp. 1165-1172, July 1988.
- [7] J. Tang, R. Zeng, H. Ma., J. He, J. Zhao, X. Li and Q. Wang, "Analysis of electromagnetic interference on dc line from parallel AC line in close proximity," *IEEE Trans. Power Delivery*, vol. 22, no. 4, pp. 2401-2408, October 2007.

- [8] N. Chopra, A.M. Gole, J. Chand, R.W. Haywood, "Zero sequence currents in ac lines caused by transients in adjacent dc lines," *IEEE Trans. Power Delivery*, vol. 3, no. 4, pp. 1873-1879, October 1988.
- [9] T. Arro, and O. Silavwe, "Coupling of transients in HVDC lines to adjacent HVAC lines and its impact on the ac line protection," Thesis for the Master of Science (M.Sc.) degree, Division of Electrical Power Engineering, Department of Energy & Environment, Chalmers University of Technology, Göteborg, Sweden 2007.
- [10] M. Szechtman, T. Wess, C.V. Thio, "First benchmark model for HVDC control studies," *Electra no. 135*, pp 55-73, April, 1991.
- [11] G. Sarcinelli Luz, N. Felipe da Silva, "First benchmark model for HVDC controls in ATP program," presented at X Symposium of specialists in electric operational and expansion planning, Florianópolis (SC), Brasil, May, 2006.
- [12] Canadian/American EMTD User Group: ATP Rule Book, distributed by the European EMTD-ATP Users Group Association, 2007.
- [13] A. Agdemir, M. Kizilcay, "Modelling of bipolar ± 500 kV HVDC system using EMTD-ATP and ATPDraw," presented at the EEUG 2008 Conference, Izmir, Turkey, September 2008 (<http://www.eeug.de/>).
- [14] Darwish H.A., Izzularab M.A., Elkashy N.I., "Enhanced Commutation Circuit Design of hvdc Circuit Breaker Using EMTD," *Transmission and Distribution Conference and Exhibition, 2005/2006 IEEE PES*, pp 978 – 985, May 2006.
- [15] M. Kizilcay, G. Bán, L. Prikler, P. Handl, "Interaction of the Secondary Arc with the Transmission System during Single-Phase Autoreclosure," *IEEE Bologna Power Tech Conf. Proceedings*, Bologna, Italy, June 2003.
- [16] M. Kizilcay, K.-H. Koch, "Numerical fault arc simulation based on power arc tests", *ETEP Journal*, vol. 4, no. 3, pp. 177-186, May/June 1994.
- [17] M. Kizilcay, P. La Seta, "Digital simulation of fault arcs in medium-voltage distribution networks," 15th Power Systems Computation Conference, 22-26 August 2005, Liège, Belgium.
- [18] A.T. Johns, R.K. Aggarwal, Y.H. Song, "Improved Techniques for Modeling Fault Arcs on Faulted EHV Transmission System", *Proc. IEE – Generation, Transmission and Distribution*, vol. 141, no. 2, pp. 148-154, March 1994
- [19] Woodford D., "Secondary Arc Effects in AC/DC Hybrid Transmission," *IEEE Trans. Power Delivery*, vol. 8, no.2, pp. 704-710, Apr. 1993.
- [20] L. Dubé, User Guide to MODELS in ATP, 1996. (available for licensed ATP users at <http://www.eeug.org/files/secret>)

VI. BIOGRAPHIES



Mustafa Kizilcay was born in Bursa, Turkey in 1955. He received the B.Sc. degree from Middle East Technical University of Ankara in 1979, Dipl.-Ing. degree and Ph.D. degree from University of Hanover, Germany in 1985 and 1991. At present he is with the University of Siegen, Germany, holding the chair for electrical power systems as full professor. Dr. Kizilcay is winner of the literature prize of Power Engineering Society of German Electro-engineers Association (ETG-VDE) in 1994. His research fields are power system analysis, digital simulation of power system transients and dynamics, insulation-coordination and protection. He is a member of IEEE, CIGRE, VDE and VDI in Germany.



Aykut Agdemir was born in Istanbul, Turkey in 1979. He received the B.Sc. degree from Black Sea Technical University of Trabzon in 2001 and M.Sc. degree from University of Hannover, Germany in 2005. He is since 2006 research assistant at the University of Siegen, Germany, Dept. of Electrical Eng. and Computer Science.



Martin Lösing was born in Germany in 1958. He received Dipl.-Ing. degree in electrical engineering from the University of Applied Sciences Osnabrück 1984. Since 1984 he is a member of planning department at RWE Transportnetz Strom in Dortmund, Germany. He is working on power system stability and dynamics in electrical power systems.